

## Research Article

Sangeeta Rout, Vanessa N. Peters, Sangram K. Pradhan, Carl E. Bonner and Mikhail A. Noginov\*

# Emission kinetics of HITC laser dye on top of arrays of Ag nanowires

<https://doi.org/10.1515/nanoph-2021-0374>

Received July 13, 2021; accepted October 16, 2021;  
published online November 2, 2021

**Abstract:** We have grown arrays of silver nanowires in pores of anodic alumina membranes (metamaterials with hyperbolic dispersion at  $\lambda \geq 615$  nm), spin coated them with the dye-doped polymer (HITC:PMMA), and studied the rates of radiative and nonradiative relaxation as well as the concentration quenching (Förster energy transfer to acceptors). The results were compared to those obtained on top of planar Ag films and glass (control samples). The strong spatial inhomogeneity of emission kinetics recorded in different spots across the sample and strong inhibition of the concentration quenching in arrays of Ag nanowires are among the most significant findings of this study.

**Keywords:** concentration quenching; emission kinetics; Förster energy transfer; Förster radius; silver nanowires.

## 1 Introduction

Control of spontaneous emission and energy transfer are among the key functionalities of photonic materials and devices. It has been shown that metamaterials with hyperbolic dispersion (lamellar metal-dielectric structures and arrays of metallic nanowires grown in pores of alumina membranes, whose dielectric permittivities in orthogonal directions have opposite signs [1–5], have high photonic densities of states (PDOS) and, in accord with the Fermi's Golden Rule, can manipulate both rates and directionality of spontaneous emission [6, 7]. In turn, Förster energy

transfer was shown to be affected by lamellar hyperbolic metamaterials [8–10], cavities [11], metallic films [8, 12], and nanoporous random structures with sponge morphology [13]. In particular, it was shown that the same nonlocal metal-dielectric environments, which boost spontaneous emission, inhibit the energy transfer [8].

Light-matter interactions involving dielectric, metallic, and hybrid nanowires have been shown to (i) enhance energy transfer from photonic nanowires to plasmonic nanowires (for applications in optical interconnects) [14], (ii) enhance the emission of quantum-dot-doped polymeric fibers by gold nanorods (for quantum emitters) [15], and (iii) enable asymmetric excitation of hybrid (MoS<sub>2</sub>:polymer) waveguides [16] and make possible other functionalities including nano-routing, high-resolution color image sensors, photovoltaics, and displays [17]. Although energy transfer studies have been carried out in multiple geometries [18, 19], including lamellar stacks of metallic and dielectric layers [8, 20], ordered nanowire array morphologies (although addressed in the literature [21]) seem to be grossly overlooked.

In order to fill the gap in the knowledge of the energy transfer in nanowire-based hyperbolic metamaterials, we studied the effect of arrays of silver nanowires on the concentration quenching of HITC dye molecules and compared the results with those obtained in different metal-dielectric environments as well as available theoretical models. The strong inhibition of the concentration quenching in arrays of Ag nanowires and large spatial inhomogeneity of emission kinetics recorded in different spots across the sample are among the most significant findings of this study.

## 2 Experimental samples and methods

The substrates used in our studies included: (i) arrays of Ag nanowires grown in pores of anodic alumina membranes, Figure 1, (ii) Ag films deposited (using thermal evaporation)

\*Corresponding author: Mikhail A. Noginov, Center for Materials, Research, Norfolk State University, Norfolk, VA 23504, USA, E-mail: mnoginov@nsu.edu

Sangeeta Rout, Vanessa N. Peters, Sangram K. Pradhan and Carl E. Bonner, Center for Materials, Research, Norfolk State University, Norfolk, VA 23504, USA. <https://orcid.org/0000-0002-6538-9489> (S. Rout)

onto glass substrates, and (iii) glass (reference samples). Self-standing 50  $\mu\text{m}$  thick alumina membranes, obtained from Redox Inc., had open  $35 \pm 5$  nm (in diameter) pores extending from wall to wall of the membrane samples, perpendicular to the surfaces. They were used to grow arrays of Ag nanowires, employing the electrodeposition technique, as discussed below. (According to our previous studies [22, 23], arrays of 35 nm nanowires, grown in membranes fabricated by the same manufacturer, have high quality and small (subwavelength) size of the unit cell, which is required for metamaterials with hyperbolic dispersion. At the same time, 50  $\mu\text{m}$  thick membranes are self-standing and convenient to work with.)

As the first step, a thin (50 nm) layer of silver was deposited on one side of an alumina membrane, using a thermal vacuum evaporator (Nano 36, from Kurt J. Lesker). In the electrodeposition experiment, the silver-coated alumina membrane served as a working electrode, while the platinum wire was used as a counter electrode, see Figure 1(a). (Platinum is a noble metal that is highly stable, inert, and resistant to corrosion and oxidation. Combined with high electrical conductivity, these properties make it a material of choice for counter electrodes used in many electrochemical reactions [24, 25].) A mixture of an aqueous solution of silver nitrate (1.50 M) and boric acid (0.4 M) buffered with nitric acid to a pH of 2–3 was used as an electrolyte. The DC voltage of  $-0.5$  V was applied during the electrodeposition process to the working electrode for 1 h. After electrodeposition, the silver film was removed (by polishing) from the backside of the membrane that was later used in the reflection measurements.

The field emission scanning electron microscopy images, depicting surface and cross-sectional morphology of the samples, along with silver nanowires grown in the membranes' pores, are shown in Figure 1(b) and (c). The measured diameters of grown nanowires,  $40 \pm 6$  nm, match (within the experimental error) those of the membrane's pores,  $35 \pm 5$  nm, suggesting that close to the samples' surface, probed in the reflection experiments, Ag fills voids completely. The majority of grown wires (83%) were longer than 1  $\mu\text{m}$ , providing for efficient light–matter coupling at p polarization [22, 26]. The surface roughness was better than  $\sim 10$  nm.

The dye-doped polymeric films were fabricated by dissolving HITC laser dye (2-[7-(1,3-Dihydro-1,3,3-trimethyl-2H-indol-2-ylidene)-1,3,5-heptatrienyl]-1,3,3-trimethyl-3H-indolium iodide) and PMMA polymer (poly(methyl methacrylate) in a dichloromethane solvent, with dye concentrations  $n = 9.5$  g/l and  $n = 24.6$  g/l (in solid state, when solvent evaporates). The prepared solutions were spin coated onto the substrates discussed above using a 6800 Spin Coater (from Specialty Coating Systems). We cautiously assume that the dye-doped polymer partly penetrated in the membranes' channels (alongside Ag) and partly resided on the samples' surface. The characteristic thickness of the dye-doped polymeric films on top of the glass and smooth Ag films, measured, using a stylus profilometer (Dektak XT from Bruker), were equal to  $80 \pm 5$  nm.

In accord with Ref. [20], the absorption and excitation spectra of HITC:PMMA films on glass have their maxima at 762 nm, while the emission spectra have the maxima at 772 nm, Figure 2.

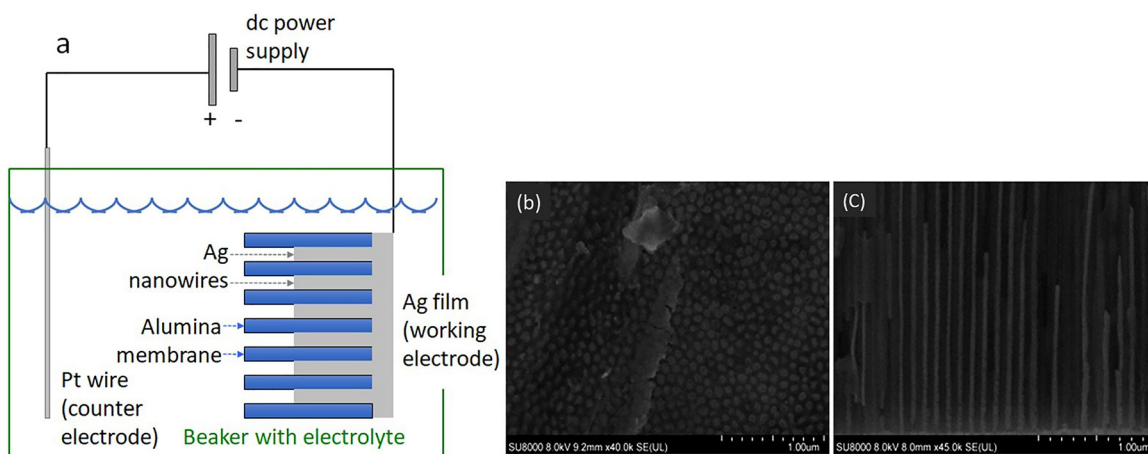


**Figure 1:** Experimental samples (a) Schematic of the electrodeposition setup. Surface (b) and cross-sectional (c) images of the alumina membrane with grown silver nanowires, obtained using field emission scanning electron microscope (FESEM SU8010 from Hitachi). In the process of electrodeposition, the surface imaged in (b), and the upper ends of the wires depicted in (c) were facing the electrolyte.

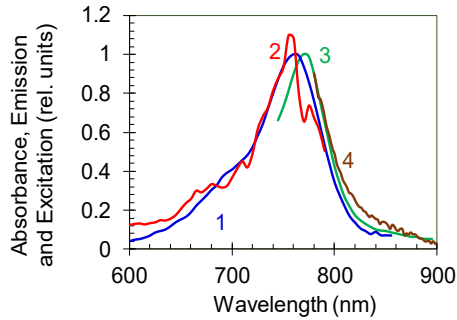


**Figure 2:** Absorption, excitation, and cw emission spectra of HITC:PMMA dye on the glass substrate with concentration equals 8.5 g/l. Trace 1 – absorption, trace 2 – excitation, trace 3 – cw emission, and trace 4 – emission spectrum measured at short-pulse pumping. Adapted from ref [20].

The p polarized reflection spectra of the arrays of silver nanowires grown in pores of alumina membranes had two maxima, Figure 3(a). The spectral position of the first peak, at  $\sim 350$  nm (ascribed to Transverse Surface Plasmon Resonance in metallic nanowires [27]), was angle-independent, while the second one, at  $\sim 600$  nm (attributed to the Epsilon Near Zero [ENZ] regime) [27], moved slightly to shorter wavelengths with an increase of the angle. The latter behavior is in a qualitative agreement with that demonstrated in the absorption spectra of arrays of Au nanorods grown in alumina membranes in Ref. [27]. The theoretically predicted wavelength positions of the second peak match the experiment at the filling factor of silver  $f \approx 0.15$ , Figure 3(b). The latter value corresponds to the filling factor of pores in alumina membranes specified by the manufacturer. This suggests a good quality of the fabricated arrays of Ag nanowires, in which silver (in a thin

layer that was probed in the reflection experiment) filled the pores almost completely Figure 1(c).

[In the calculations above, we first computed the spectra of the effective medias' dielectric permittivities in the directions parallel and perpendicular to Ag nanowires [28], indicating that the regime of hyperbolic dispersion (at which dielectric permittivities in orthogonal directions have opposite signs) occurs at  $\lambda \geq 615$  nm. After this, we substituted the numbers to the analytical formula for the angular and wavelength-dependent reflection of a uniaxial medium derived in Ref. [22]. Multiple spectral positions of the reflection maxima, calculated at different metal filling factors  $f$ , are plotted in Figure 3(b) as the function of the incidence angle, along with the experimental data points.]

## 3 Results and discussion

### 3.1 Emission kinetics measurements

In the emission kinetics experiments, HITC:PMMA films, deposited on top of fabricated arrays of silver nanowires (described above), Ag films, and glass substrates were excited at  $\lambda = 795$  nm with  $\sim 150$  fs pulses of a 76 MHz mode-locked Ti:sapphire laser (Mira 900 from Coherent). The laser beam was loosely focused into a 2.5 mm spot, and the average laser power on the sample was  $\sim 60$  mW. The emission kinetics were recorded (at  $\lambda \geq 850$  nm) using the visible and near-infrared Streak Camera (Model C5680 from Hamamatsu) equipped with long-pass color filters. The width of the recorded laser pulse, determined by the jitter of the laser and wide-open entrance slit of the streak camera, was equal to  $\sim 100$  ps.

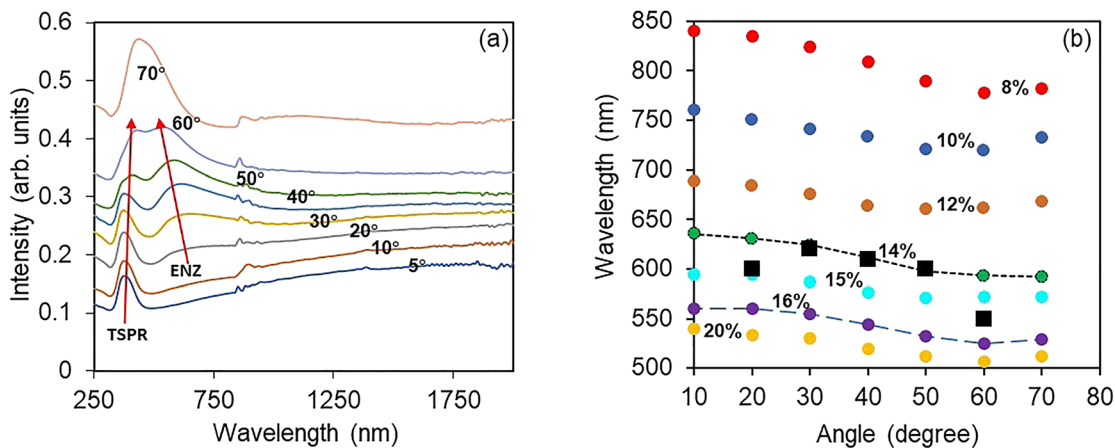


**Figure 3:** Reflection and dispersion (a) Reflection spectra of arrays of Ag nanowires grown in pores of alumina membrane taken in p polarization at different incidence angles. (b) Dependence of the ENZ reflection maximum on the incidence angle. Large black squares – experiment, other sets of characters – calculations are done at different filling factors  $f$  shown in the figure.

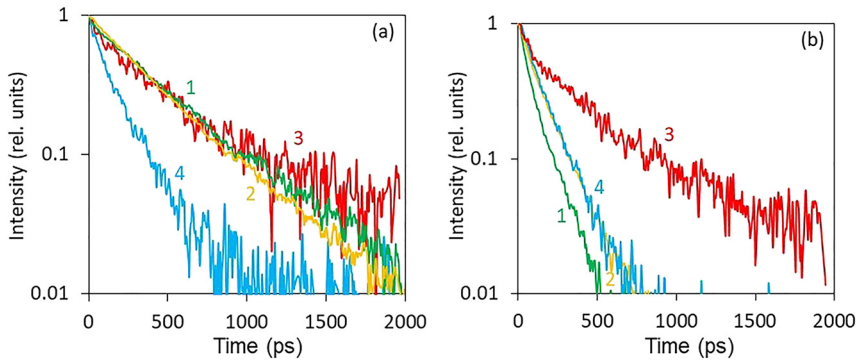


**Figure 4:** Emission kinetics (a) Emission kinetics of HITC:PMMA film at modest dye concentration  $n = 9.5$  g/l deposited on glass (green trace 1), smooth Ag films (yellow trace 2), and arrays of Ag nanowires: red trace 3 corresponds to the upper boundary of the emission kinetics spread, while blue trace 4 corresponds to its lower boundary. (b) Same for high dye concentration  $n = 24.6$  g/l.

The emission kinetics of HITC:PMMA films with modest dye concentration ( $n = 9.5$  g/l), deposited on glass, were relatively long and nearly single exponential, Figure 4(a). However, at the larger dye concentration ( $n = 24.6$  g/l), the emission kinetics shortened significantly and deviated from the exponential function, Figure 4(b). According to Ref. [20], the latter behavior is due to a concentration quenching Förster energy transfer to quenching centers. If emission kinetics are approximated by exponential functions, the decay rates can be derived and fitted with the formula  $\sim(A + W) + \gamma n^2$ , where  $A$  and  $W$  are the rates of radiative and nonradiative (e.g. vibrational) decay, and  $\gamma n^2$  is the effective rate of the energy transfer [20]. The latter term is insignificant at low dye concentrations and becomes predominant at large values of  $n$ .

The emission kinetics of the same HITC:PMMA films deposited on smooth Ag films are depicted in Figure 4(a) and (b) (traces 2). At  $n = 9.5$  g/l (relatively small concentration quenching), the emission kinetics were almost similar to those on top of the glass, Figure 4(a). At the same time, at large dye concentration,  $n = 24.6$  g/l, the emission kinetics (still fast in comparison to that at  $n = 9.5$  g/l) slowed down relative to that on glass, manifesting inhibition of the concentration quenching in the vicinity to metal (traces 1 and 2 in Figure 4(b)), in agreement with Ref. [20].

The emission kinetics obtained in HITC:PMMA films deposited onto arrays of Ag nanowires were highly

inhomogeneous. Thus, the emission kinetics recorded (at both dye concentrations) in different local spots on the samples showed a large spread of the decay rates, Figure 5(a) and (b). The characteristic lateral scale of the emission nonuniformity (effective sizes of domains with more or less homogeneous kinetics) was  $\sim 1$  mm. This behavior is similar to that observed in nanoporous Au foam substrates impregnated with HITC:PMMA [13]. At the same time, such spreads of emission kinetics were never observed on top of the glass, smooth metallic films, or alumina membranes without deposited metallic nanowires.

Red and blue solid traces in Figure 5(a) and (b) correspond to the upper and the lower boundaries of the emission kinetic spreads in HITC:PMMA films deposited onto arrays of Ag nanowires grown in pores of alumina substrates. These boundary traces are plotted in Figure 4(a) and (b) together with the emission kinetics recorded on top of the glass and smooth Au film substrates. The corresponding decay rates are summarized in Figure 6.

As it was stated above [20], the emission decay rate  $D$  is given by:

$$D = (A + W) + \gamma n^2,$$

where  $(A + W)$  is the substrate-dependent rate of radiative and nonradiative relaxation (including energy transfer to metal in metal-based substrates),  $\gamma n^2$  is the substrate-

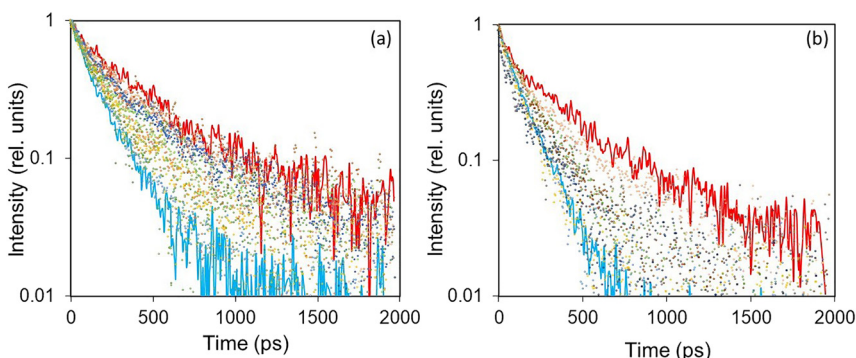


**Figure 5:** Spread of emission kinetics in HITC:PMMA films deposited on top of arrays of Ag nanowires in alumina membranes at dye concentrations  $n = 9.5$  g/l (a) and  $n = 24.6$  g/l (b). Red and blue solid lines indicate the upper and the lower boundaries of the emission kinetics spreads, respectively.

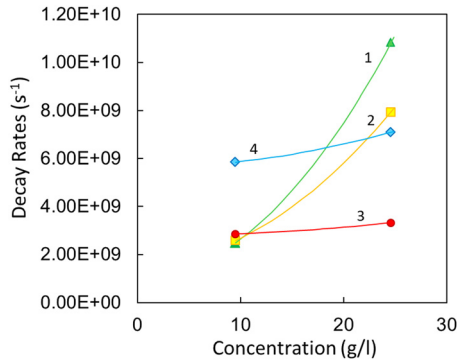


**Figure 6:** Emission decay rates for HITC:PMMA films at two different dye concentrations,  $n = 9.5$  g/l and  $n = 24.6$  g/l, on top of the glass (trace 1, green triangles), smooth Ag films (trace 2, yellow squares), and arrays of Ag nanowires: Upper boundary of the kinetics spread (trace 3, red circles) and lower boundary of the kinetics spread (trace 4, blue diamonds). The solid lines were calculated using the determined parameters  $A + W$  and  $\gamma$ .

dependent concentration quenching rate, and  $n$  is the dye concentration. For each substrate studied, we measured two emission decay rates  $D$  ( $D_1$  and  $D_2$ ) at two dye concentrations  $n$  ( $n_1 = 9.5$  g/l and  $n_2 = 24.6$  g/l). The resulting system of two equations with two unknown values was solved to yield  $(A + W)$  and  $\gamma$ . The values  $(A + W)$ ,  $\gamma n_1^2$ , and  $\gamma n_2^2$ , derived for four types of kinetics studied, on top of the glass (1), on top of Ag film (2), and on top of arrays of Ag nanowires (corresponding to the upper (3) and the lower (4) boundaries of the kinetics spreads) are depicted in Figure 7 and the calculated curves  $(A + W) + \gamma n^2$  (obtained by varying  $n$ ) are plotted in Figure 6.

One can see that, as one gradually moves from sample 1 to sample 4, the decay rate  $(A + W)$  increases, Figure 7. In

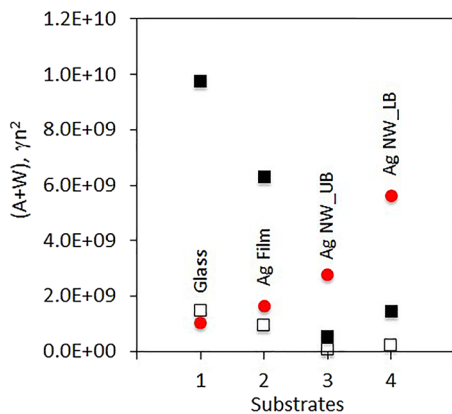


**Figure 7:** Decay rates  $A + W$  (red circles) and  $\gamma n^2$ , calculated at  $n = 9.5$  g/l (open squares) and  $n = 24.6$  g/l (solid squares) on top of the glass (1, glass), on top of Ag film (2, Ag film), and on top of arrays of Ag nanowires, close to the upper boundary (3, Ag NW\_UB) and the lower boundary (4, Ag NW\_LB) of the kinetics spreads.

hyperbolic metamaterials (alumina membranes with Ag nanowires) this can be due to an increase of the PDOS and corresponding enhancement of the spontaneous emission rate  $A$ . At the same time, in silver-based samples, the increase of the nonradiative relaxation rate can be due to an enhancement of the energy transfer to metal, which appears to be larger in arrays of Ag nanowires than in smooth silver film samples. The latter difference can be due to (i) the large surface area of Ag nanowires and/or (ii) the small distance between dye molecules and metal if dye penetrates into pores with already deposited silver nanowires.

While the concentration quenching at high dye concentration,  $n = 24.6$  g/l, was the predominant mechanism of excitation relaxation on top of the glass, it reduced strongly in presence of metal, in particular on top of arrays of Ag nanowires. At the same time, at smaller dye concentration,  $n = 9.5$  g/l, the concentration quenching rate  $\gamma n^2$  was modest on top of the glass and became insignificant on top of alumina membranes impregnated with silver nanowires, Figure 7. The reduction of the concentration quenching rate in metal-based samples can have two possible explanations: (i) reduction of the Förster radius (caused by the energy transfer to metal) and corresponding inhibition of the concentration quenching [29], and (ii) effective reduction of the dye concentration and increase of intermolecular distances, if dye molecules penetrate in pores of the membranes. The latter phenomenon was observed in dye-impregnated alumina membranes without metal [30]. The same inhibition mechanism should also be possible in membranes with Ag nanowires grown in the pores. However, it requires penetration of the dye molecules to membranes pores, and it is not clear whether this was the case with our silver-filled membranes.

## 4 Summary

*To summarize*, we have grown arrays of silver nanowires in pores of anodic alumina membranes (metamaterials with hyperbolic dispersion at  $\lambda \geq 615$  nm), spin coated them with the dye-doped polymer HITC:PMMA, and studied the rates of radiative and nonradiative relaxation as well as the concentration quenching (Förster energy transfer to acceptors). The results were compared to those obtained on top of smooth Ag films and control substrates (glass).

In agreement with Ref. [20], the emission kinetics on top of glass shortened with an increase of the dye concentration. This is a manifestation of concentration quenching Förster energy transfer to acceptors. The concentration quenching is getting inhibited on top of silver

substrates. According to Ref. [29], this phenomenon can be explained by reduction of the Förster radius, caused by energy transfer to metal, and corresponding slowing down of the donor-acceptor energy transfer.

The emission kinetics recorded on top of arrays of Ag nanowires grown in pores of anodic alumina membranes were highly inhomogeneous. Correspondingly, the decay rates measured in different local spots on the samples were strongly different from each other. The physical mechanism of the large inhomogeneity of the emission kinetics is not completely understood. We infer that the coupling of dye molecules with arrays of Ag nanowires is weaker or stronger in different local spots, which can be due to nonuniform distribution of the diameters of Ag nanowires, the distance between them, and average dye molecule-to-nanowire distances. This effect was recently observed in dye-doped Au nanofoam samples (scattering sponge-like structures) [13] but never seen in scattering alumina membranes without metallic nanowires or on top of smooth metallic or dielectric substrates.

We described the emission decay rate as  $D = (A + W) + \gamma n^2$  [20] and determined values  $(A + W)$  and  $\gamma n^2$  for four types of kinetics studied: on top of the glass (1), on top of Ag film (2), and on top of arrays of Ag nanowires (corresponding to the upper (3) and lower (4) boundaries of the emission kinetics spreads). As one gradually moves from sample 1 to sample 4, the decay rates  $(A + W)$  increase, while the rates of the energy transfer  $\gamma n^2$  decrease. This result is in agreement with that previously reported in both hyperbolic and not hyperbolic substrates [8]. Therefore, it is not directly tied to the hyperbolicity of the dispersion curves.

We infer that the increase of  $(A + W)$  is primarily due to the energy transfer to metal, which is larger in arrays of Ag nanowires than in-plane silver film samples. The latter difference can be due to (i) the large surface area of Ag nanowires and/or (ii) the small distance between dye molecules and metal if dye penetrates into pores with deposited silver nanowires.

The inhibition of concentration quenching in metal-based and porous samples can have two possible reasons: (i) reduction of the Förster radius (caused by the energy transfer to metal) and a corresponding decrease of the energy transfer [29], and (ii) effective lessening of the dye concentration and increase of intermolecular distances, if dye molecules penetrate in the membrane's pores [30].

**Author contributions:** All the authors have accepted responsibility for the entire content of this submitted manuscript and approved submission.

**Research funding:** The work was supported in part by NSF grants 1830886, and 1856515, AFOSR grant FA9550-18-1-0417, and DoD grant W911NF1810472.

**Conflict of interest statement:** The authors declare no conflicts of interest regarding this article.

## References

- [1] A. Poddubny, I. Iorsh, P. Belov, and Y. Kivshar, "Hyperbolic metamaterials," *Nat. Photonics*, vol. 7, pp. 948–957, 2013.
- [2] P. A. Belov, "Backward waves and negative refraction in uniaxial dielectrics with negative dielectric permittivity along the anisotropy axis," *Microw. Opt. Technol. Lett.*, vol. 37, pp. 259–263, 2003.
- [3] D. R. Smith and D. Schurig, "Electromagnetic wave propagation in media with indefinite permittivity and permeability tensors," *Phys. Rev. Lett.*, vol. 90, p. 077405, 2003.
- [4] A. Salandrino and N. Engheta, "Far-field subdiffraction optical microscopy using metamaterial crystals: theory and simulations," *Phys. Rev. B*, vol. 74, p. 075103, 2006.
- [5] Z. Jacob, L. V. Alekseyev, and E. Narimanov, "Optical hyperlens: far-field imaging beyond the diffraction limit," *Opt. Express*, vol. 14, pp. 8247–8256, 2006.
- [6] Z. Jacob, I. I. Smolyaninov, and E. E. Narimanov, "Broadband purcell effect: radiative decay engineering with metamaterials," *Appl. Phys. Lett.*, vol. 100, p. 181105, 2012.
- [7] H. N. S. Krishnamoorthy, Z. Jacob, E. Narimanov, I. Kretzschmar, and V. M. Menon, "Topological transitions in metamaterials," *Science*, vol. 336, pp. 205–209, 2012.
- [8] T. U. Tumkur, J. K. Kitur, C. E. Bonner, A. N. Poddubny, E. E. Narimanov, and M. A. Noginov, "Control of Förster energy transfer in the vicinity of metallic surfaces and hyperbolic metamaterials," *Faraday Discuss.*, vol. 178, pp. 395–412, 2015.
- [9] D. J. Roth, M. E. Nasir, P. Ginzburg, et al., "Forster resonance energy transfer inside hyperbolic metamaterials," *ACS Photonics*, vol. 5, pp. 4594–4603, 2018.
- [10] W. D. Newman, C. L. Cortes, A. Afshar, et al., "Observation of long-range dipole–dipole interactions in hyperbolic metamaterials," *Sci. Adv.*, vol. 4, p. eaar5278, 2018.
- [11] P. Andrew and W. L. Barnes, "Forster energy transfer in an optical microcavity," *Science*, vol. 290, pp. 785–788, 2000.
- [12] C. Blum, N. Zijlstra, A. Lagendijk, et al., "Nanophotonic control of the Förster resonance energy transfer efficiency," *Phys. Rev. Lett.*, vol. 109, p. 203601, 2012.
- [13] S. Rout, Z. Qi, L. S. Petrosyan, et al., "Effect of random nanostructured metallic environments on spontaneous emission of HITC dye," *Nanomaterials*, vol. 10, p. 2135, 2020.
- [14] X. Yang, Y. Li, Z. Lou, Q. Chen, and B. Li, "Optical energy transfer from photonic nanowire to plasmonic nanowire," *ACS Appl. Energy Mater.*, vol. 1, pp. 278–283, 2018.
- [15] X. Yang, R. Xu, D. Bao, and B. Li, "Gold nanorod-enhanced light emission in quantum-dot-doped polymer nanofibers," *ACS Appl. Mater. Interfaces*, vol. 6, pp. 11846–11850, 2014.
- [16] X. Yang, L. Wen, J. Yan, et al., "Energy dissipation and asymmetric excitation in hybrid waveguides for routing and coloring," *J. Phys. Chem. Lett.*, vol. 12, pp. 7034–7040, 2021.

- [17] M. Chen, L. Wen, D. Pan, D. R. S. Cumming, X. Yang, and Q. Chen, "Full-color nanorouter for high-resolution imaging," *Nanoscale*, vol. 13, pp. 13024–13029, 2021.
- [18] P. G. Wu and L. Brand, "Resonance energy transfer: methods and applications," *Anal. Biochem.*, vol. 218, pp. 1–13, 1994.
- [19] X. Liu and J. Qiu, "Recent advances in energy transfer in bulk and nanoscale luminescent materials: from spectroscopy to applications," *Chem. Soc. Rev.*, vol. 44, pp. 8714–8746, 2015.
- [20] S. Prayakarao, S. R. Koutsares, C. E. Bonner, and M. A. Noginov, "Effect of nonlocal metal–dielectric environments on concentration quenching of HITC dye," *J. Opt. Soc. Am. B*, vol. 36, pp. 3579–3587, 2019.
- [21] D. J. Roth, M. E. Nasir, P. Ginzburg, et al., "Förster resonance energy transfer inside hyperbolic metamaterials," *ACS Photonics*, vol. 5, pp. 4594–4603, 2018.
- [22] M. A. Noginov, Y. A. Barnakov, G. Zhu, T. Tumkur, H. Li, and E. E. Narimanov, "Bulk photonic metamaterial with hyperbolic dispersion," *Appl. Phys. Lett.*, vol. 94, p. 151105, 2009.
- [23] M. A. Noginov, H. Li, Y. A. Barnakov, et al., "Controlling spontaneous emission with metamaterials," *Opt. Lett.*, vol. 35, pp. 1863–1865, 2010.
- [24] J. Wu, Z. Lan, J. Lin, et al., "Counter electrodes in dye-sensitized solar cells," *Chem. Soc. Rev.*, vol. 46, pp. 5975–6023, 2017.
- [25] Y. L. Lee, C. L. Chen, L. W. Chong, C. H. Chen, Y. F. Liu, and C. F. Chi, "A platinum counter electrode with high electrochemical activity and high transparency for dye-sensitized solar cells," *Electrochem. Commun.*, vol. 12, pp. 1662–1665, 2010.
- [26] L. V. Alekseyev, E. E. Narimanov, T. Tumkur, H. Li, Y. A. Barnakov, and M. A. Noginov, "Uniaxial epsilon-near-zero metamaterial for angular filtering and polarization control," *Appl. Phys. Lett.*, vol. 97, p. 131107, 2010.
- [27] R. J. Pollard, A. Murphy, W. R. Hendren, et al., "Optical nonlocalities and additional waves in epsilon-near-zero metamaterials," *Phys. Rev. Lett.*, vol. 102, p. 127405, 2009.
- [28] J. Elser, R. Wangberg, V. A. Podolskiy, and E. E. Narimanov, "Nanowire metamaterials with extreme optical anisotropy," *Appl. Phys. Lett.*, vol. 89, p. 261102, 2006.
- [29] S. Koutsares, L. S. Petrosyan, S. Prayakarao, et al., "Effect of metallic substrates and cavities on emission kinetics of dye-doped polymeric films," *J. Opt. Soc. Am. B*, vol. 38, pp. 88–94, 2021.
- [30] S. Rout, S. R. Koutsares, D. Courtwright, et al., "Effect of nanoscale dielectric environments on concentration quenching," *Nanophotonics*, vol. 10, no. 14, pp. 3659–3665, 2021.